ACADEMIA ENGINEERING

Research Article
Published: 2025-06-25
https://doi.org/10.20935/AcadEng7756

A second-generation non-invasive brain–computer interface (BCI) design for wheelchair control

Nicoladie D. Tam[1,*]

Academic Editor: Vítor Carvalho

Abstract

A hands-free, wearable brain–computer interface (BCI) with fault tolerance is proposed for individuals with quadriplegia, enabling safe wheelchair control. It anticipates operational failures with fault-recovery methods to mitigate catastrophic outcomes. A multimodal system validates decoded signals for sensor consistency and confirms user intentions. The primary imaging system utilizes optical sensors to monitor brain signals, while a supplementary system employs accelerometers and gyroscopes to detect head movements. A third subsystem recognizes voice commands via built-in microphones. The primary control decodes the direction of movement, and the secondary confirms this through head tilting. A third redundancy uses voice commands to confirm or override wheelchair operations. Although cumbersome, head movements and voice commands are essential for users who are paralyzed and unable to press buttons in emergencies. Head motion sensors also detect headset slippage, halting operations immediately in the event of a headset drop. An adaptive voting system employing a majority-rule method filters out inconsistent outliers by utilizing historical patterns of consistency in the weight-sum voting process. To validate the interpretation of optical data collected from brain signals in the prefrontal cortex (PFC) using functional near-infrared spectroscopy (fNIRS), motor task experiments were conducted with human subjects performing horizontal hand movements in four orthogonal directions. The results indicated that oxy-hemoglobin (oxy-Hb) and deoxy-hemoglobin (deoxy-Hb) signals exhibited directional specificity, with responses reversing during opposing movements. It suggests that neural activity reflects the direction of movement. The consistency of the decoded results is verified by hemodynamic variables, with oxy-Hb and deoxy-Hb signals covarying inversely. Phase relationships between hemodynamic variables also changed depending on the direction of movement. An analysis revealed that the dynamics of vasodilation and vasoconstriction varied, indicating conditions where the oxygen supply could not meet metabolic demand in specific movement directions. The design allows users to choose a lightweight headband for cost-effective PFC monitoring or a helmet for whole-brain signal detection. The wearable design also provides wireless or wired headset options for communication with the controller located on the wheelchair. Future developments will address headset slippage challenges through adaptive signal processing, ensuring the commercial viability and reliability of the product.

Keywords: *neural signal processing, fNIRS (functional near-infrared spectroscopy), hemodynamic analysis, fault-tolerant engineering design, neuroprosthetics, phase-space analysis*

Citation: Tam ND. A second-generation non-invasive brain–computer interface (BCI) design for wheelchair control. *Academia Engineering* 2025;2. https://doi.org/10.20935/AcadEng7756

1. Introduction

A second-generation brain–computer interface (BCI) device for wheelchair control is proposed to demonstrate the feasibility of using non-invasive optical brain signals to decode movement direction. Experimental evidence will support the interpretation of hemodynamic signals to validate accuracy, without relying on an ad hoc feature-extraction algorithm often deemed physiologically uninterpretable. Independent hemodynamic variables effectively validate movement intentions. Both oxy-Hb and deoxy-Hb hemodynamic responses can represent movement direction, while their phase relationships confirm these intentions. Neuro-responses (represented by deoxy-Hb levels), cardio responses (represented by oxy-Hb levels), and the dynamics of oxygen supply provide redundant metrics to validate physiological representations. This second-generation design addresses operational issues to mitigate catastrophic failure, rather than focusing solely on the accuracy concerns of first-generation devices. It integrates sensors from multiple modalities for redundancy, incorporating head motion detection and voice commands to confirm or cancel unintentional operations. A majority-rule voting scheme is employed for consistency checking, as congruent signals are more likely to be accurate than inconsistent ones.

Additionally, endpoint specification simplifies control by eliminating the need for continual updates to the path trajectory from brain signals, thereby delegating path planning and obstacle avoidance to a semi-autonomous navigation subsystem. The device offers a choice between a lightweight headband for prefrontal cortex (PFC) recording and a helmet-based whole-brain headset for enhanced user adoption. The wearable device separates lightweight headset sensors from the heavier controller on the wheelchair via wireless or wired communication. However, practical issues such as sensor slippage must be addressed before commercializing the device.

[1]Department of Biological Sciences, University of North Texas, Denton, TX 76203, USA.
*email: nicoladie.tam@unt.edu

1.1. First-generation brain–computer interface designs with microelectrode implants

Recent advancements in multi-electrode recording techniques have demonstrated that neurons in the primary motor cortex (M1) can compute vector sums to decode movement directions [1–7]. Each neuron fires most effectively in its preferred direction and contributes to movement by firing at a rate corresponding to the vector projection at that angle. The resulting movement is defined by the population vector, the vector sum of the neural firings [7, 8]. It has been demonstrated that a robotic arm can be controlled by brain signals recorded using implanted microelectrodes [9]. The first-generation BCI device utilized motor cortex neuron firing rates to control robotic arm movements [10]. It decoded neural responses by computing the vector sum to determine the intended movement direction.

1.1.1. Neural population vector representation of movement direction

The population vector hypothesis suggests that neural firing rates collectively encode the intended direction of movement. Each neuron fires most strongly in its preferred direction, diminishing its firing rate in other directions. Thus, firing rates act as a vector in polar coordinates, peaking at the preferred angle and varying according to the cosine projection. The vector sum of the firing rates from all participating neurons indicates the intended direction of movement. When a neuron fires uniformly across all movement directions, it encodes only magnitude as a scalar.

In contrast, varying firing rates according to direction adds a movement-related aspect. According to the cosine tuning function, a neuron that fires maximally in one direction while decreasing in others represents a vector with both magnitude and direction. This projection encodes the angle; however, symmetric angles may create ambiguity, which can be resolved through the vector sum of other neurons. The overall direction corresponds to the angle in the resultant vector sum, which can be determined by downstream neurons from the resultant firing vector sum [11]. Knowing all neurons' preferred directions and firing rates allows us to predict the intended direction from the vector sum. A BCI can similarly infer movement direction using the resultant vector sum; however, detecting firing rates requires invasive microelectrode implants or other non-invasive techniques.

Decoding movement requires microelectrode implants to monitor approximately 100 cortical neurons. Brain movement can cause electrodes to become unstable, leading to signal loss. Discriminating neuron firings necessitate specialized neural expertise. Limited biocompatibility raises safety concerns. Graphene's flexibility may offer a durable, biocompatible alternative to metal electrodes, thereby enhancing the performance of implanted electrodes [12–14]. Graphene nanoelectrodes present a promising option for neural recording [15]. However, many paralyzed patients avoid implants due to infection risks, which limits the adoption of first-generation neuroprosthetic BCI devices.

1.1.2. Brain–computer interface designs using EEG or ECoG electrodes

Electroencephalogram (EEG) signals are used non-invasively to detect brain activity for BCI devices [16]. However, a low signal-to-noise ratio caused by skull filtering and limited spatial resolution restricts the practical applications of this method. Microvolt-range EEG signals are highly susceptible to external noise, reflecting cumulative field potentials rather than the firing rates of individual neurons. An increase in field potential does not indicate a higher firing rate; it often represents synchronized firing, especially during seizures. Nevertheless, EEG signals can identify the focal source of epileptic seizures based on synchronized activities [17, 18]. High-density EEG, utilizing 128 to 256 EEG electrodes, can localize synchronized signal sources [19], as validated by structural MRI [20].

Most EEG-based BCIs utilize motor imagery paradigms [21] to link neural signals with motor activity for feature detection and classification [22]. The classified features in the frequency domain often relate to muscle activation, such as the opening and closing of orthotic limbs using actuators [23] for discrete intentions, rather than decoding movement directions, as in population firing vector representation. It is crucial to control a wheelchair's movement direction using a 360° angle instead of on/off signals or ad hoc methods, which can extract features without accounting for the physiological encoding of neural firings, such as vector firing projections. Neurofeedback can enhance BCI functionality to improve the extracted representations, for instance, by combining EEG and fMRI (functional magnetic resonance imaging) [24]. However, this increases the weight and size of BCI sensors, and MRI machines may be too heavy for mobile wheelchair control. An electrocorticogram (ECoG) offers a superior signal-to-noise ratio compared to EEG by placing electrodes directly on the cortical surface [25, 26]. However, placement requires brain surgery. A 32-electrode ECoG has been demonstrated to control 3D cursor movements [27], but most people avoid neurosurgery unless it is necessary to locate seizure sources.

1.1.3. Brain–computer interface designs using magnetic signals

Magnetic signals can non-invasively detect brain activity. Functional magnetic resonance imaging (fMRI) identifies paramagnetic deoxy-hemoglobin (deoxy-Hb) through blood-oxygen-level-dependent (BOLD) signals, which indicate neurovascular coupling related to blood flow, oxygenation, and metabolism. The roles of astrocytes, pericytes, and neurons in regulating brain blood flow remain unclear [28]. Deoxy-Hb levels rise in response to neural activity, reflecting metabolic demand and indirectly indicating neural firing [29]. However, oxy-Hb cannot be magnetically detected. Magnetic imaging thus captures contributions to oxygenation. The Results section will demonstrate that additional oxy-Hb signals enhance movement direction decoding beyond those of deoxy-Hb signals. The temporal resolution of fMRI limits the functionality of real-time BCI for wheelchair control, as scans last one second and require users to remain still. Moreover, wheelchair movements may interfere with the operation, even if the magnets are miniaturized. Additionally, MRI machines are too bulky and expensive for mobile BCI applications, making alternative imaging methods more practical.

1.2. Brain–computer interface designs using optical signals

Optical imaging provides a non-invasive method for detecting brain signals that reflect neural firing rates, similar to fMRI. This principle relies on the modified Beer–Lambert law (mBLL) [30, 31] to identify variations in oxy-Hb and deoxy-Hb levels within tissues.

Using the deoxy-Hb signal is analogous to the BOLD signal in fMRI for detecting neural activity, serving as a proxy for oxygen extraction from Hb during increased metabolic activity resulting from neural firing. Near-infrared light (NIR) penetrates tissues, making it particularly suitable for imaging the brain. If neural responses are specific to the direction of movement, these hemodynamic signals can be employed to decode intended movements for BCI-controlled wheelchairs.

Fingertip oximeters exemplify the use of optical imaging in medical devices. These monitors measure pulse rate and blood oxygen levels by detecting hemoglobin absorption through a finger using infrared or visible light [32]. The emitter and detector are positioned on opposite sides of the fingertip to analyze light absorption. Photoplethysmography measures changes in oxy-Hb and deoxy-Hb levels based on their light absorption characteristics, similar to optical brain imaging, which detects hemodynamic signals to infer neural activity. Pulse rate is based on variations in oxy-Hb levels.

Meanwhile, blood oxygen saturation (SpO2) is the ratio of oxy-Hb to the blood volume, as indicated by the sum of oxy-Hb and deoxy-Hb [33]. These oximeters are a routine optical imaging technology that provides reliable measurements in medical photoplethysmography [34]. Utilizing dependable technology reinforces the acceptance of optical imaging as a trusted device.

1.2.1. Hemodynamic representation of neural activity

Functional near-infrared spectroscopy (fNIRS) detects brain signals using NIR light, similar to fingertip oximeters [35–39]. Optodes are lightweight sensors used in mobile BCI headsets. fNIRS employs absorption spectroscopy by directing light onto the tissue and identifying the molecular content through the absorption spectrum. It detects oxy-Hb and deoxy-Hb levels for hemodynamic analyses. While fMRI relies on a single hemodynamic deoxy-Hb signal, fNIRS improves BCI design by utilizing both the deoxy-Hb and oxy-Hb signals. The dynamics of oxygen supply and metabolic demand also reveal changes in neural representation during movement, as shown below.

1.2.2. Non-invasive design requirements for optical brain imaging

The design specifications for non-invasive optical brain imaging require positioning emitter–detector pairs on the scalp without needing probe insertion. Ray tracing utilizes light-scattering physics to facilitate this process, as light refracts back to the scalp's surface due to scattering. Scattered light follows a banana-shaped path, returning to the emitter surface [30, 40] (see **Figure 1**). Emitter–detector pairs can monitor brain signals optically from absorption along the light path. This methodology is employed in most commercially available fNIRS instruments. Computations convert optical density to concentration changes using the mBLL, which is incorporated into the hardware–software optical imaging system.

The depth of the light path depends on the distance between the emitter and detector. Greater distances facilitate deeper tissue detection, but scattered noise limits this depth to 2–3 cm from the scalp surface [38, 41, 42]. The noise restrictions enable optical recordings to detect cortical activity. However, deep-brain activity can be predicted with 70% accuracy, as validated by fMRI co-registration [39]. Fortunately, cortical signals are sufficient for movement decoding, particularly from the primary motor cortex, premotor cortex, supplementary motor cortex, or PFC, which involve motor execution, planning, bilateral coordination, and decision making for movement intentions.

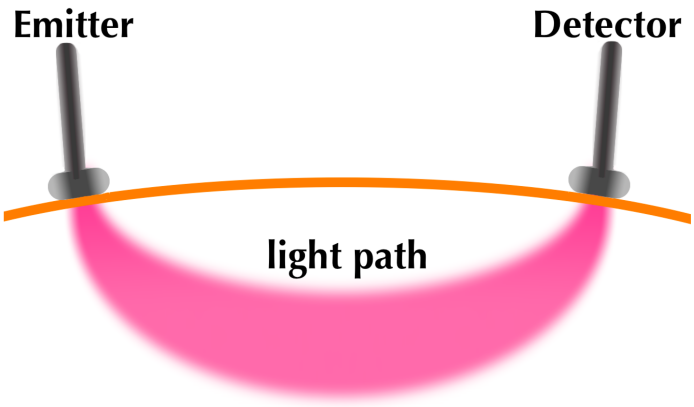

Figure 1 • The diagram illustrates light traveling along a curved path to the surface of the emitter, creating a banana-shaped light trajectory without a detector probe positioned within the tissue. This method enables non-invasive brain imaging using emitter–detector pairs placed on the surface of the scalp.

1.2.3. Brain–computer interface experimental designs

Most fNIRS BCI experiments focus on motor imagery and cognitive tasks for feature extraction rather than on movement angles [43]. Additionally, they often combine fNIRS with EEG to enhance neural signals [44, 45], relying on various signals for validation instead of solely optical signals. Most fNIRS BCIs use motor imagery tasks, which cannot validate fictive movements without physical activity. Furthermore, these tasks often require the suppression of real movements, which can potentially diminish neural signals. Gait control experiments aid motor rehabilitation but lack evidence for predicting movement directions [46]. Finger-tapping tasks classify go or no-go signals without defining movement angles. Although these tasks [47, 48] can tackle signal analysis, movement direction is continuous, not discrete.

Other BCI studies on PFC activity predict executive functions. Thus, it is challenging to validate neural representations without confirming accurate movement execution. through cognitive or emotional tasks, such as mental workload [49], emotional valence [50], or impulsivity, rather than motor intentions [51]. This study employs a real hand movement task to identify directionality and link it to neural representations, allowing for unrestricted physical movements. Patients with spinal cord injuries can generate brain signals for motor control, even if those signals do not reach their limbs. Therefore, wheelchair control tasks should involve actual horizontal movements toward intended endpoints for validation, correlating them with neural signal representations to ensure physiological accuracy.

2. Second-generation BCI design specifications

2.1. A reliable wearable design with redundancy for fault recovery

The second-generation BCI design decodes brain signals for wheelchair control using a redundant multi-sensor approach,

which minimizes catastrophic failures from component malfunctions and decoding errors. It utilizes physiologically interpretable neural signals to validate movements. Unlike first-generation devices, this hands-free design for users with paralysis prioritizes managing component failures over decoding accuracy, as quadriplegic users cannot press an emergency button if the device slips or falls. The design incorporates built-in failure-detection mechanisms for effective error management and recovery.

To enhance versatility, it should be a lightweight, wearable device that detects brain signals non-invasively, eliminating the need for surgery or implants. It must operate using a fail-safe methodology to prevent accidents and alleviate anxiety. To cut costs, it uses off-the-shelf components instead of custom designs. It should be user-friendly to encourage broader adoption, requiring minimal effort or training. The minimum specifications are as follows:

1. Non-invasive neural signal detection;
2. Mobile, lightweight, wearable, and detachable device;
3. Multiple independent brain signal variables for validation;
4. Integrated multimodal sensor technologies with brain signals for redundant control;
5. A fault-tolerant system capable of recovering from faults while exhibiting graceful degradation;
6. A trusted, proven technology ensuring reliable operations;
7. The utilization of commercially available components for cost-effectiveness.

2.2. Utilizing multiple independent and derived brain signal variables for control

Experimental evidence will be provided to differentiate the movement direction for wheelchair control as proof of concept. Various analytical methods will redundantly decode brain signals, using hemodynamic variables to validate wheelchair operations. These variables include, but are not limited to:

- The oxy-Hb variable (Δ [HbO]) is used to assess the cardiovascular responses related to oxygen delivery and availability.
- The deoxy-Hb variable (Δ [Hb]) is used to determine neuro-responses related to oxygen extraction, provided sufficient oxygen is available.

The physiological interpretations of derived variables from the original hemodynamic variables include:

- Variables representing the combined amount of oxy-Hb and deoxy-Hb indicate the total blood volume, which is used to identify responses related to vasodilation and vasoconstriction;
- Phase relationship variables between oxy-Hb and deoxy-Hb (representing the time-lag and time-lead responses);
- The hemodynamic ratio of oxy-Hb to deoxy-Hb represents the relative amount of oxygen availability, indicating whether conditions are in surplus or deficit and highlighting the dynamics of oxygen supply and demand.

The Results sections below illustrate how these independent and derived hemodynamic variables are utilized to validate and confirm the accuracy of the decoded movement directions as redundant measures for consistency checks. They demonstrate the application of multiple methodologies for decoding direction from these variables, serving as proof of concept for wheelchair control.

2.3. Multi-sensor redundancy consistency check for reliable operation

Good engineering design acknowledges that component failures occur due to normal wear and tear, thereby mitigating the risks of catastrophic failure through fault recovery. Utilizing multiple sensors and hemodynamic variables ensures accuracy through consistency checking. It integrates a multi-sensor system with optical signals, head movements, and voice commands for redundancy. The system verifies movement direction through brain signals and head tilt, while the primary control decodes the intended movement using optical signals confirmed by head motions. Voice commands clarify intentions and serve as a panic button for quadriplegic users who are unable to push a button physically. They can override errors and abort unintentional wheelchair operations during emergencies.

This fault-tolerant design reduces catastrophic failures by gradually degrading functions. It employs a majority-rule voting system to mitigate sensor inconsistencies and background noise. This method assumes accuracy over outliers, dismissing inconsistencies as invalid. It utilizes a weighted voting scheme to ensure consistent outcomes while enhancing accuracy and minimizing errors. It resembles adaptive neural network learning in adjusting weights, accompanied by a verification scheme to prevent error propagation. The consistency-checking system resolves ambient noise, interference, and crosstalk issues by rejecting outliers and inconsistent signals. Noises are non-signals unrelated to brain or head tilt motion. Contaminated brain signals are treated as non-signals and are automatically rejected by the system.

Commercial voice recognition systems enable user-specific speech detection without requiring extensive development. If the system fails to recognize a voice due to interference during emergencies, any voice command can override all operations and shut it down, rendering signal interference irrelevant. The system continuously monitors brain signals but interprets them on demand for wheelchair control. It does not require the constant decoding of brain signals for semi-autonomous navigation. Interference from subsystems during non-decoding periods is irrelevant, since they only activate in response to user commands to alter navigation.

2.4. Interchangeable options for wearable helmets and headband headsets

The current design offers various headset sensor versions, providing users with options based on cost and convenience. The full version includes a helmet-mounted headset with embedded optodes that monitor brain signals while blocking ambient infrared light. It fits better and allows for precise sensor positioning. However, hair affects NIR light absorption; darker hair absorbs more light, which reduces optical brain signals. Alternatively, the headband is a lightweight option worn on the forehead. It detects PFC signals without interference from hair, ensuring optical quality. It is more affordable than the helmet version but has fewer brain signal sensors.

The headset features an optical sensor, accelerometer, and microphone for voice recognition. The accelerometer and gyroscope track head motion and function as shock sensors. It connects to the wheelchair's BCI controller wirelessly or through a wired connection. The wireless version requires a battery, while the wired option communicates via tethered wires and supplies power. The removable design relocates heavy components to the wheelchair's BCI controller, enabling versatility with interchangeable options, including a helmet or headband, suitable for wired or wireless communication.

2.5. A schematic diagram of the BCI device

A schematic diagram (**Figure 2**) illustrates the block diagram of the subsystem components for the BCI device. It shows a detachable headset, a BCI controller, and a wheelchair navigation controller subsystem. The headset wirelessly communicates with the BCI controller for signal processing and wheelchair control, functioning as a helmet for whole-brain monitoring or as a headband for PFC activity. Alternatively, a tethered wired option is available to eliminate the need for a battery on the headset. It includes sensors for recording optical signals and detecting head motion, and a microphone for voice recognition and analysis. The BCI controller, mounted on the wheelchair, manages signal processing and control. Battery packs power the headset and controllers, while the wheelchair navigation controller interprets signals from the BCI controller to operate the wheelchair.

2.6. User-friendly semi-autonomous system design

A semi-autonomous design reduces user effort by utilizing autopilot for wheelchair navigation, eliminating the need for detailed driving instructions. It minimizes brain signal misinterpretation by specifying endpoints instead of updating intermediate steps. This motor control mimics cerebellum functions, enabling fluid coordination without extensive control directives. The autopilot manages path planning and obstacle avoidance, allowing users to focus on movement without complex navigational instructions, making it more straightforward than BCI-controlled 3D robotic arms.

2.7. Adaptive control design for sensor slippage

The system must adapt to brain signals over time to compensate for inaccurate detection caused by sensor slippage. Biofeedback calibrates sensor signals to brain control, particularly during initial training phases. The headset's motion detector detects slippage caused by rapid acceleration or deceleration. It detects drops through shock sensors that measure sudden g-forces, employing impulse and jerk functions to assess rapid deceleration changes.

Optical sensors detect brain signals from specific locations, so repositioning them captures signals from different areas. The decoding algorithm adjusts for this shift. Adaptive decoding recovers from errors. When decoding is vetoed due to inconsistencies, it may indicate headset slippage, regardless of the accelerometer's detection. The system must recalibrate to ensure accurate signal interpretation.

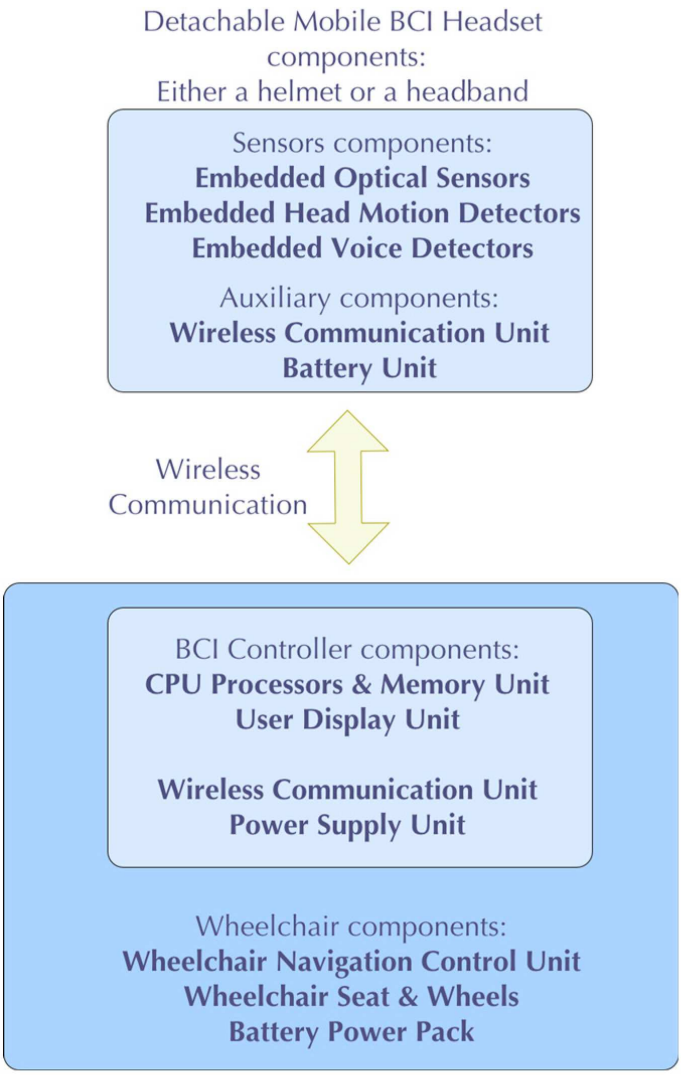

Figure 2 • A schematic diagram of the wheelchair BCI device features a headset, similar to a helmet or headband, equipped with sensors for optical signals, head movements, and voice commands. It includes a wireless unit with a battery that communicates with the BCI controller on the wheelchair, which contains navigation controls and a battery pack.

3. Methods

3.1. Experimental methods

3.1.1. Orthogonal direction motor tasks

Human subjects were recruited to perform a motor task while recording optical brain signals to assess neural representations of movement directions. The task involved executing arm movements across a desk surface (see **Figure 3**). Participants moved their dominant hands in right–left or front–back directions, indicating movement intentions along the x-axis and y-axis on a horizontal plane, which is relevant for controlling a wheelchair. Alternate right and left movements occurred in each trial, signaled by a sound cue (see **Figure 3**). Front and back movements were performed in separate trials, corresponding to neural responses that decoded intended movements. This repeated movement paradigm facilitates event-triggered signal averaging in subsequent analyses.

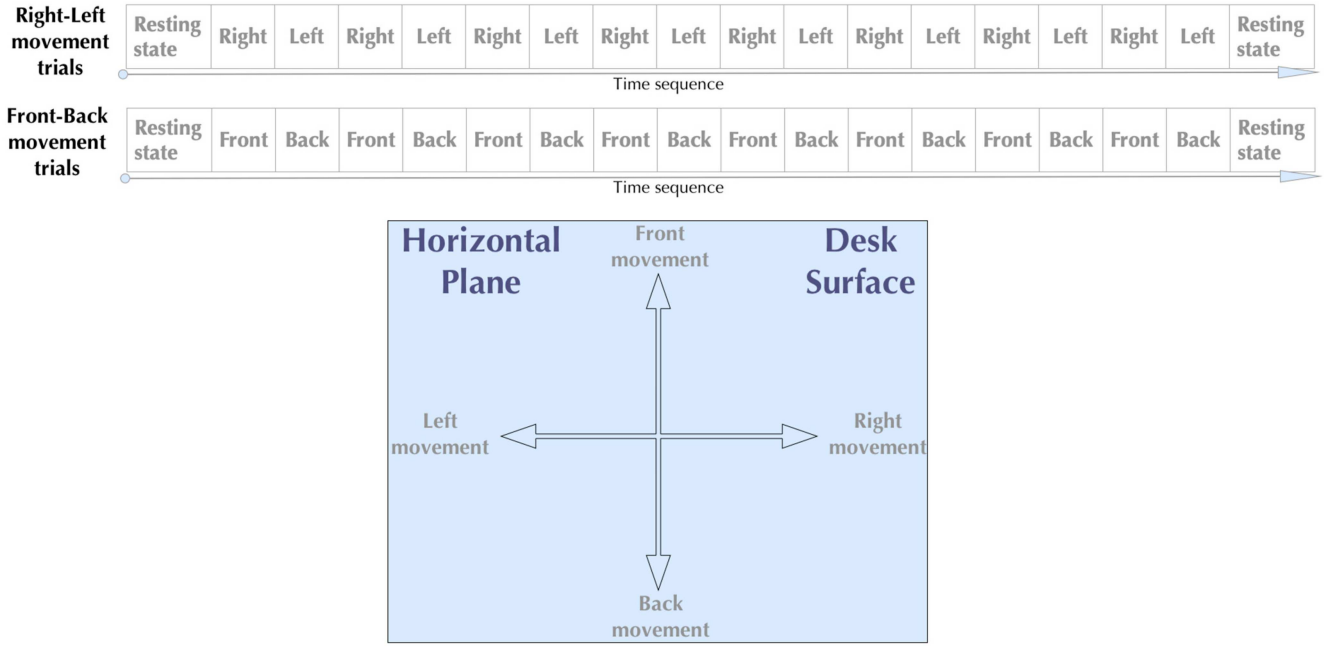

Figure 3 • The diagram illustrates the protocol for the motor tasks (top panels). A sound tone signaled the onset of movement. The bottom panel shows the horizontal desk surface used for the trials. Right–left and front–back movements were recorded with optical signals synchronized with sound cues.

Subjects moved their hands 30 cm across the desk, pausing for cues for the next movement. The tone repeated every 4.3 s for a total of two minutes. Orthogonal directions streamlined the experiment, enabling the inference of diagonal movements from firing vector projections using the vector sum encoding hypothesis. If a center-out task [3–7] were used, it would require returning to the starting point before the subsequent trial; however, this return is not counted due to the off-center origin. Since movement directions are independent of origin, this approach reduces the number of experimental trials by half using alternating opposing-direction movements instead of the center-out design.

3.1.2. Simultaneous optical signal recordings

Simultaneous optical brain imaging was conducted during motor tasks using the fNIRS Imagent™ from ISS, Inc., Champaign, IL, USA Fiber optic cables transmitted 690 and 830 nm wavelengths to the headsets, digitizing the signals at a rate of 10 Hz across 64 channels. The system converts optical density signals into two hemodynamic time series (oxy-Hb and deoxy-Hb) while recording synchronized movement event markers. The headset employs concentric circles of emitters and detectors to image brain regions of interest (ROIs). Other vendors offer compact headsets featuring LED emitters arranged in rectilinear grids, which facilitate the detection of multiple brain locations. This LED design eliminates the need for tethered fiber optic cables, allowing for wireless or wired transmission to the processing unit. The proposed BCI headset will utilize the wireless LED option as a mobile device. The Imagent™ headset features concentric circle emitters and detectors to target specific brain regions.

The PFC was selected for this experiment due to its comfortable fit on the forehead, which minimizes signal loss caused by hair interference. Subjects remained stationary for five seconds before and after each trial to establish a baseline of brain activity and relaxed before the subsequent trial. The Institutional Review Board (IRB) approved the protocol, and participants signed informed consent. The data were anonymized to protect the subjects' identities. A total of 96 healthy college-aged individuals, including both males and females, participated.

3.2. Analytical methods

3.2.1. Signal preprocessing

Hemodynamic data were preprocessed using a moving average to reduce noise. Physiological signals exhibit serial correlation and gradual changes. A moving average smooths abrupt fluctuations while preserving the similarity of sequential data points. This method relies on the principle that sequential trends are serially related, while noise is serially independent. It minimizes artificial alterations to the original signal by assuming and filtering specific bandwidths as noise.

An offset is added to achieve a zero mean, facilitating the interpretation of responses as activation or deactivation. Activations are positive values indicating increases, while deactivations are negative values representing decreases. Since the dataset is based on a calibrated reference level from the start of the experiment using mBLL, adding an offset does not affect the relative temporal changes in the signal. This offset enables BCI decoding algorithms to automatically characterize responses.

3.2.2. Identifying physiological responses

Decoding brain signals requires identifying specific physiological responses. Mapping signal features to classifications or utilizing an artificial intelligence (AI) classifier may aid BCI control; however, these methods lack physiological interpretability. A reliable BCI device decodes interpretable physical phenomena rather than relying on arbitrary mappings from brain signals to wheelchair control. Thus, the goal is to detect physiological responses from available optical signals. Identifying relevant physiological responses is crucial for decoding brain signals. Using a classifier to map features or applying AI for BCI control lacks the necessary interpretability for

validation. A reliable device should deliver interpretable decoding of physical phenomena, not merely map data to control a wheelchair. Therefore, this study aims to identify decodable physiological responses.

3.2.3. Time-series analysis

Time-series analysis examines hemodynamic signals that change over time. A response shows deviations from a specific baseline. A trend refers to non-random variations in a consistent direction over time, which can reflect physiological responses. Trend analysis identifies these changes by determining their onset and endpoint. Cumulative sum (CUSUM) analysis detects trends in non-random deviations from a baseline [52]. It identifies serially correlated patterns and establishes dependence statistics over time. The criteria focus on consecutive non-random changes, revealing trends obscured by noise fluctuations while remaining within normal levels. This method successfully identifies significant trends when sequential changes are non-random. CUSUM statistics were initially developed to detect faulty batches in manufacturing quality control due to consecutive failures in parts [52]. Trends are identified by sliding a V-shaped control chart along the increasing cumulative sum function.

CUSUM slope analysis detects trends using a moving window based on the slope [53]. Noise, being serially independent, results in random fluctuations that offset each other, leading to a zero. Sequential variations in the same direction cause the slope to deviate from zero, increasing or decreasing in response to those changes. While the CUSUM slope remains a non-monotonic function for noise, significant monotonic deviations from zero indicate the onset of a trend, while a return to zero signifies its end [53]. This method eliminates the need for a sliding control chart and automates the detection of the BCI device's movement direction.

3.2.4. Scalar sum signal analysis

Optical signals detect neural activity from deoxy-Hb, capturing collective rather than individual firings. Unlike extracellular recordings of action potentials, hemodynamic signals reflect a weighted average of group firings along the light path. A population vector requires both magnitude and direction for decoding, but optical signals detect only magnitude. If neurons in a group have randomly distributed preferred directions, their scalar sum may cancel. However, if group firing indicates their preferred direction without cancelation, adjacent neurons likely process similar directional information. If the group firing of optical signals is movement-direction specific, then it may represent a vector rather than a scalar sum that is direction-specific. The Results section demonstrates that hemodynamic responses are directionally specific, confirming that clusters of neurons process movement in a directionally consistent manner. Downstream neurons or BCI devices could decode movement direction based on the vector sum.

3.2.5. Oxygen supply and demand analysis

Hemodynamic signals detect changes in oxy-Hb and deoxy-Hb during motor tasks, revealing the dynamics of oxygen supply and demand. These metrics are often inversely related; as demand rises, oxygen extraction increases, leading to higher deoxy-Hb and lower oxy-Hb levels. Oxygen supply typically lags, illustrating the phase relationship between oxy-Hb and deoxy-Hb and their shifts in response to the direction of movement.

The relationship between oxy-Hb and deoxy-Hb relies on a constant total oxygen blood supply, which may not hold during peak metabolic activity when the supply is insufficient. Both levels decrease, altering their relationship from inverse to direct. If this occurs during movement, it indicates an extreme oxygen demand and helps detect direction. Phase-space analysis can identify this transition, providing a method to confirm movement direction from hemodynamic variables for BCI decoding algorithms.

3.2.6. Phase-space analysis

A phase-space plot graphically displays the covarying relationships between two time series $x(t)$ and $y(t)$ based on their quadrant locations (x, y) [54, 55]. For hemodynamic analysis, the two time series are $x = \Delta[\mathrm{HbO}]$ and $y = \Delta[\mathrm{Hb}]$, denoted by brackets to indicate concentration. A phase-space plot illustrates the evolving relationship over time through its trajectory [56]. It identifies the specific relationships between the $\Delta[\mathrm{HbO}]$ and $\Delta[\mathrm{Hb}]$ variables, including proportionality, phase relationships, and time lead/lag according to quadrant position. Additionally, the hemodynamic ratio $\Delta[\mathrm{HbO}]/\Delta[\mathrm{Hb}]$ quantitatively describes changes in covariation, providing another variable for the BCI decoding algorithm to validate movement direction.

The first quadrant $(+x, +y)$ shows both variables increasing positively along a diagonal. The third quadrant $(-x, -y)$ indicates that both variables decrease simultaneously, demonstrating negative covariation. The second quadrant $(-x, +y)$ reveals an inverse relationship: as one variable increases, the other decreases. The fourth quadrant $(+x, -y)$ similarly shows that as one variable increases, the other decreases, reflecting another inverse relationship. Changes in movement direction can alter the covarying hemodynamic relationships, quantified by the phase-space quadrant that the trajectory traverses (see further details below).

The shape of the trajectory reveals the phase relationship and oxygen delivery delays during the extraction of neural tissue. If oxy-Hb and deoxy-Hb change in sync, the trajectory appears as a line. A time lead or lag results in an elliptical or circular path; more significant deviations indicate longer delays. Movement-related phases can be quantified by trajectory deviations from the negative diagonal.

In a zero-mean adjusted time series, data points center around the origin $(0, 0)$ of the phase space, dividing the phase relationships into four quadrants. The negative diagonal trajectories reveal inversely proportional relationships. Typically, the hemodynamic variables $\Delta[\mathrm{HbO}]$ and $\Delta[\mathrm{Hb}]$ are coupled: an increase in oxygen consumption leads to a decrease in supply, as indicated by a negative diagonal trajectory. This negative diagonal line $\Delta[\mathrm{HbO}] = -\Delta[\mathrm{Hb}]$ divides the phase space into upper and lower regions, representing the hemodynamic ratio $r(t) = \Delta[\mathrm{HbO}] / \Delta[\mathrm{Hb}] = -1$ for movement direction decoding if the covarying relationship changes with direction.

3.2.7. Zero-sum hemodynamics

If blood flow is constant, it exhibits a zero-sum response $\Delta[\mathrm{HbO}] + \Delta[\mathrm{Hb}] = 0$ when the changes are equal and opposite $\Delta[\mathrm{HbO}] = -\Delta[\mathrm{Hb}]$. This relationship occurs in aerobic metabolism when

the oxygen supply meets demand, represented by the negative diagonal. Total blood volume can vary in one direction while remaining constant in another. This negative diagonal line divides the phase space: trajectories below show oxy-Hb changes exceeding deoxy-Hb when $\Delta[\mathrm{HbO}] < -\Delta[\mathrm{Hb}]$. Trajectories above the diagonal quantify the converse. Suppose blood flow is constant in one direction but varies due to vasoconstriction or vasodilation in another. In that case, zero-sum hemodynamics can measure these differences using the phase-space quadrant, the slope of the negative diagonal, and the hemodynamic ratio.

Oxygen availability depends on delivery and extraction levels. A surplus occurs when the delivered oxygen exceeds the extraction when $\Delta[\mathrm{HbO}] > \Delta[\mathrm{Hb}]$, which is indicated by trajectories located below the negative diagonal in phase space. However, lower extraction does not always signify a surplus; it can result from insufficient availability, as extraction cannot exceed what is available during a bottleneck. Therefore, reduced extraction may reflect a deficit rather than a surplus. Thus, an additional condition is the magnitude needed to differentiate between a surplus and a deficit. The slope of the diagonal trajectory determines the magnitude of the phase-space difference.

Oxygen surplus occurs only when both conditions $\Delta[\mathrm{HbO}] > \Delta[\mathrm{Hb}]$ and $|\Delta[\mathrm{HbO}]| > |\Delta[\mathrm{Hb}]|$ exist, and it is detectable by trajectories below the negative diagonal $\Delta[\mathrm{HbO}] > \Delta[\mathrm{Hb}]$ with a slope magnitude less than -1, $|\Delta[\mathrm{HbO}]| / |\Delta[\mathrm{Hb}]| < -1$. A positive change indicates a surplus, while a negative change shows a deficit.

Conversely, oxygen deficits occur when the trajectories fall below the negative diagonal and have a slope greater than -1. Furthermore, an oxygen deficit arises when demand exceeds supply, as indicated by trajectories above the negative diagonal, regardless of the magnitude $\Delta[\mathrm{HbO}] < \Delta[\mathrm{Hb}]$. This condition provides an additional measure to validate BCI decoding, specifically whether the dynamics of oxygen supply and demand are reversed in relation to movement direction. However, the BCI decoding algorithm requires two conditions.

4. Results

4.1. Movement-specific responses for BCI control

The hemodynamic responses were recorded from optode A6 on the left dorsolateral PFC (dlPFC), displaying neuro-responses (deoxy-Hb) (see **Figure 4** in blue) and cardio-responses (oxy-Hb) (see **Figure 5** in red). The graphs represent event-triggered average responses aligned with the sound tone of movement onset. To avoid ambiguity between "right hand" versus "right direction," the term "rightward" is used instead of "right" unless the context is clear.

Cumulative sum (CUSUM) trend statistics were used to detect trends from baseline noise levels [53]. A deviation of 3 standard deviations serves as the criterion for indicating significant trend deviations from the baseline noise level, which is considered a physiological response. Statistically significant trends are represented by a diamond symbol on the data points in the hemodynamic graphs in **Figure 4**, **Figure 5** and **Figure 6**. A moving window of 11 data points was used to identify a sequential trend that deviates from the noise level. Note that trends can be detected even when obscured by noise. They may fall within the noise fluctuation level; however, trends consist of consecutive changes serially correlated as significant responses.

4.2. Hemodynamic responses distinguishing right–left and front–back movements

4.2.1. Direction-specific neuro-responses

Figure 4 illustrates neuro-responses (deoxy-Hb) for right–left movements. A small but significant peak (activation) occurred during rightward movements (right graph), while a trough (deactivation) was observed during leftward movements (left graph). Their responses were inversely related: activation during rightward and deactivation during leftward movements. The analysis indicates an oxygen deficit limited the peak response during rightward movements. Hemodynamic responses could have been greater with sufficient oxygen for extraction. However, the responses remained statistically significant despite being reduced. It suggests that neuro-responses were specific to the movement direction for the BCI algorithm to decode.

In contrast, the neuro-responses in **Figure 4** for orthogonal front–back movements exhibited a continually decreasing slope for forward movements (top graph) and an increasing slope for backward movements (bottom graph). They demonstrated inverse trends, with rising patterns in one direction and decreasing patterns in the other. Responses were deactivating during forward movements and activating during backward movements.

The neuro-responses in **Figure 4** were inversely related during opposing movements and varied orthogonally across all four conditions. They peaked during rightward movements and reached a trough during leftward movements. In contrast, they gradually increase during forward movements while decreasing during backward movements. This finding shows that optical hemodynamic signals capture group responses with directional specificity, indicating that the neural group under an optode shares similar preferred directions. Despite the scalar sum signals from optodes, one can determine the firing vector when responses are direction-specific.

4.2.2. Direction-specific cardio responses

Figure 5 illustrates cardio-responses (oxy-Hb) during right–left movements, displaying peaks in oxygen delivery for leftward movements (left graph) and troughs for rightward movements (right graph). Oxygen delivery peaked during leftward movements but decreased to a minimum during rightward movements, suggesting inverse relationships for opposing directions, parallel to the opposing neuro-responses but inversely. Thus, the oxy-Hb variable can independently validate the direction decoded by deoxy-Hb. This measure complements hemodynamic data to verify movement direction for the BCI device as a consistency check.

However, cardio responses continually increased during forward movements (top graph) but gradually decreased during backward movements (bottom graph). Oxygen availability increased during forward motion and decreased during backward motion, exhibiting an inverse trend: increasing availability with forward motion versus decreasing availability with backward motion. The trends in oxygen availability (indicated by oxy-Hb) were opposite for each movement direction, highlighting direction-specific responses for non-neural hemodynamic variables in BCI movement direction decoding.

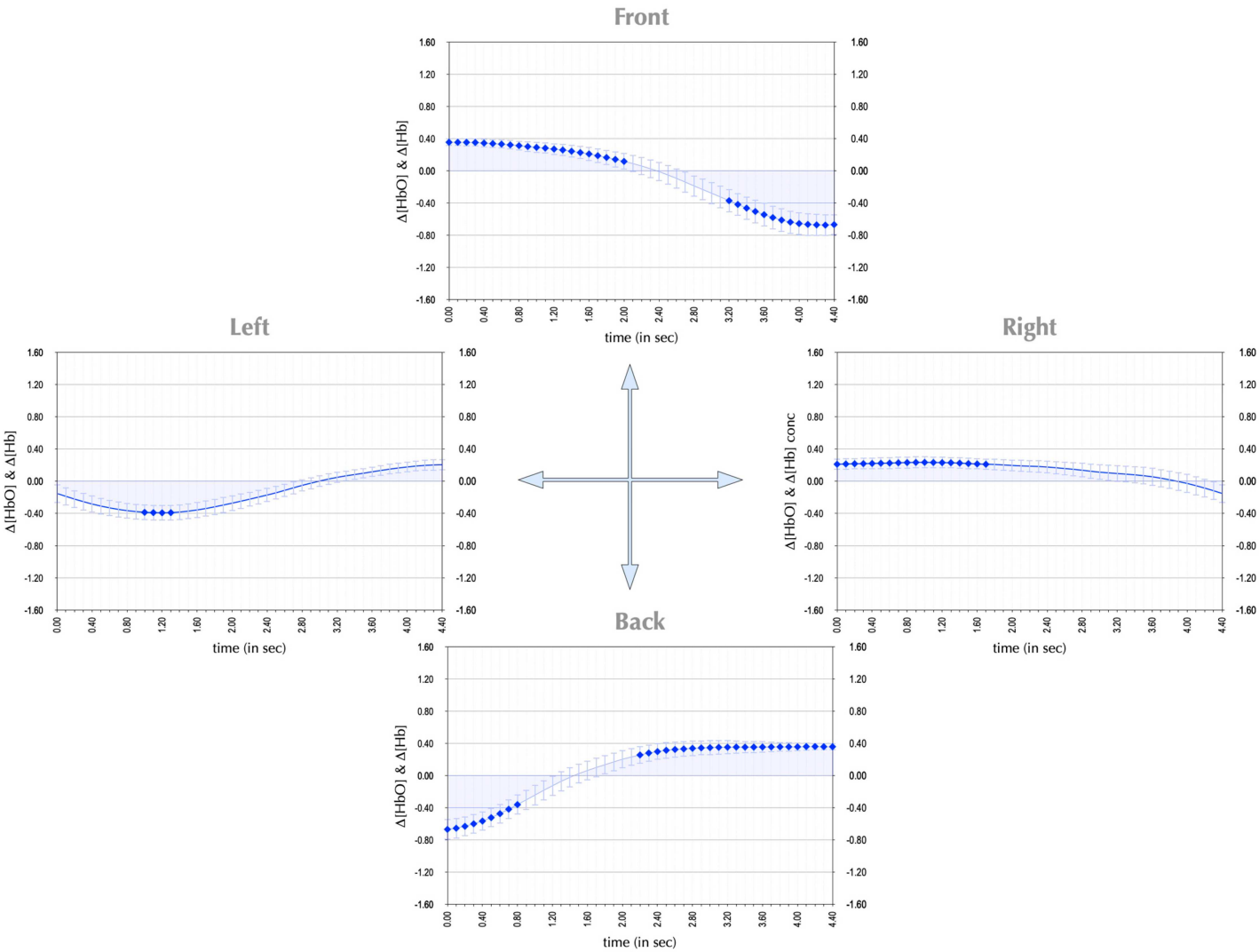

Figure 4 • Event-triggered average hemodynamic responses during right–left and front–back movements illustrate neuro-responses (deoxy-Hb levels) for optode A6 in the PFC across four directions. Movement onset aligns with the graph's origin. Responses peaked during rightward movements and were lowest during leftward movements. For front–back movements, responses decreased during forward movements and increased during backward movements. These direction-specific responses are distinguishable in both opposite and orthogonal directions. (Deoxy-Hb is shown in blue. Error bars represent standard errors. Diamond points indicate significant trends that deviate from baseline noise, based on CUSUM slope statistics.)

The cardio responses (oxy-Hb) in **Figure 5**, similar to the neuro-responses (deoxy-Hb) in **Figure 4**, exhibited distinct reactions across all movement directions. They reflected the neuro-responses, emphasizing inverse relationships. Note that oxy-Hb signals are different physiological cardio responses that can independently verify the accuracy of direction decoding based on the firing vectors of neuro-responses.

4.2.3. Coupling relationships between neuro- and cardio responses

Figure 6 illustrates the coupling between neuro- and cardio responses by combining **Figure 4** and **Figure 5**. The graphs reveal an inversely proportional relationship between changes in oxy-Hb and deoxy-Hb levels, indicating that they are coupled yet inversely related. However, neuro- and cardio responses covary with different time leads or lags depending on movement direction. Cardio responses exhibited much larger peaks (left graph) and troughs (right graph) than neuro-responses, $|\Delta\,[\mathrm{HbO}]| > |\Delta\,[\mathrm{Hb}]|$, indicating greater variation in oxygen availability for extraction. The phase relationships that varied with movement direction will be examined using phase-space analysis below to validate the accuracy of decoded movement directions as redundancy measures for consistency checking, evn though they are dependent variables.

4.2.4. Oxygen surplus and oxygen deficit during opposing direction movements

An analysis of the physiological responses revealed the oxygen supply and demand dynamics. Comparing oxygen availability (oxy-Hb) and extraction (deoxy-Hb) showed a surplus, $(\Delta\,[\mathrm{HbO}] + \Delta\,[\mathrm{Hb}]) > 0$, for leftward movements (left graph in **Figure 6**) and a deficit, $(\Delta\,[\mathrm{HbO}] + \Delta\,[\mathrm{Hb}]) < 0$, for rightward movements (right graph in **Figure 6**). A positive change, $(\Delta\,[\mathrm{HbO}] + \Delta\,[\mathrm{Hb}]) > 0$, in leftward movements is dominated by cardio responses (supply), which outpaced neuro-responses (demand), suggesting an available oxygen surplus. However, the scenario of rightward movements is inverted (right graph in **Figure 6**). Cardio responses (oxygen delivery) declined more than neuro-responses (oxygen extraction), $(\Delta\,[\mathrm{HbO}] + \Delta\,[\mathrm{Hb}]) < 0$,

indicating an oxygen deficit. The availability of oxygen decreased more rapidly than demand, which limited oxygen extraction and resulted in flattening of neuro-responses (deoxy-Hb) observed in **Figure 6**. It shows the supply and demand dynamics were directionally dependent. There was an oxygen surplus in leftward movements and a deficit in rightward movements. This finding suggests that oxygen supply and demand are not necessarily a zero-sum game under these conditions.

4.2.5. Vasodilation and vasoconstriction during opposing direction movements

To illustrate how total blood volume changes during motor tasks, **Figure 7** shows the sum of oxy-Hb and deoxy-Hb, representing the total blood volume and the overall amount of hemoglobin in the blood $\Delta[\mathrm{HbO}] + \Delta[\mathrm{Hb}]$. Leftward movements revealed vasodilation, as indicated by an increased total blood volume (a positive value). Conversely, vasoconstriction occurred during rightward movements due to a decreased in blood volume (a negative value). Blood volume change is not a zero-sum; it increased during leftward movements and decreased during rightward movements, thus differentiating between the right and left sides based on vasodilation and vasoconstriction.

4.2.6. Constant blood volume during orthogonal direction movements

In contrast, blood volume remained constant during front–back movements, showing no vasoconstriction or vasodilation (top and bottom graphs in **Figure 7**). This indicates zero-sum hemodynamic responses, unlike the non-zero-sum responses observed in the orthogonal right–left directions. This derived hemodynamic variable could validate the movement directions represented by the neuro- or cardio responses by incorporating constant blood flow, vasodilation, or vasoconstriction as additional measures, even though they are dependent variables, as their sum.

4.2.7. Direction-specific phase-space representations

The phase-space plots in **Figure 8** illustrate the phase trajectory relationships between oxy-Hb and deoxy-Hb during movement trials. They followed a negative diagonal trajectory, but their angles, shapes, locations, and trajectories varied in orthogonal directions.

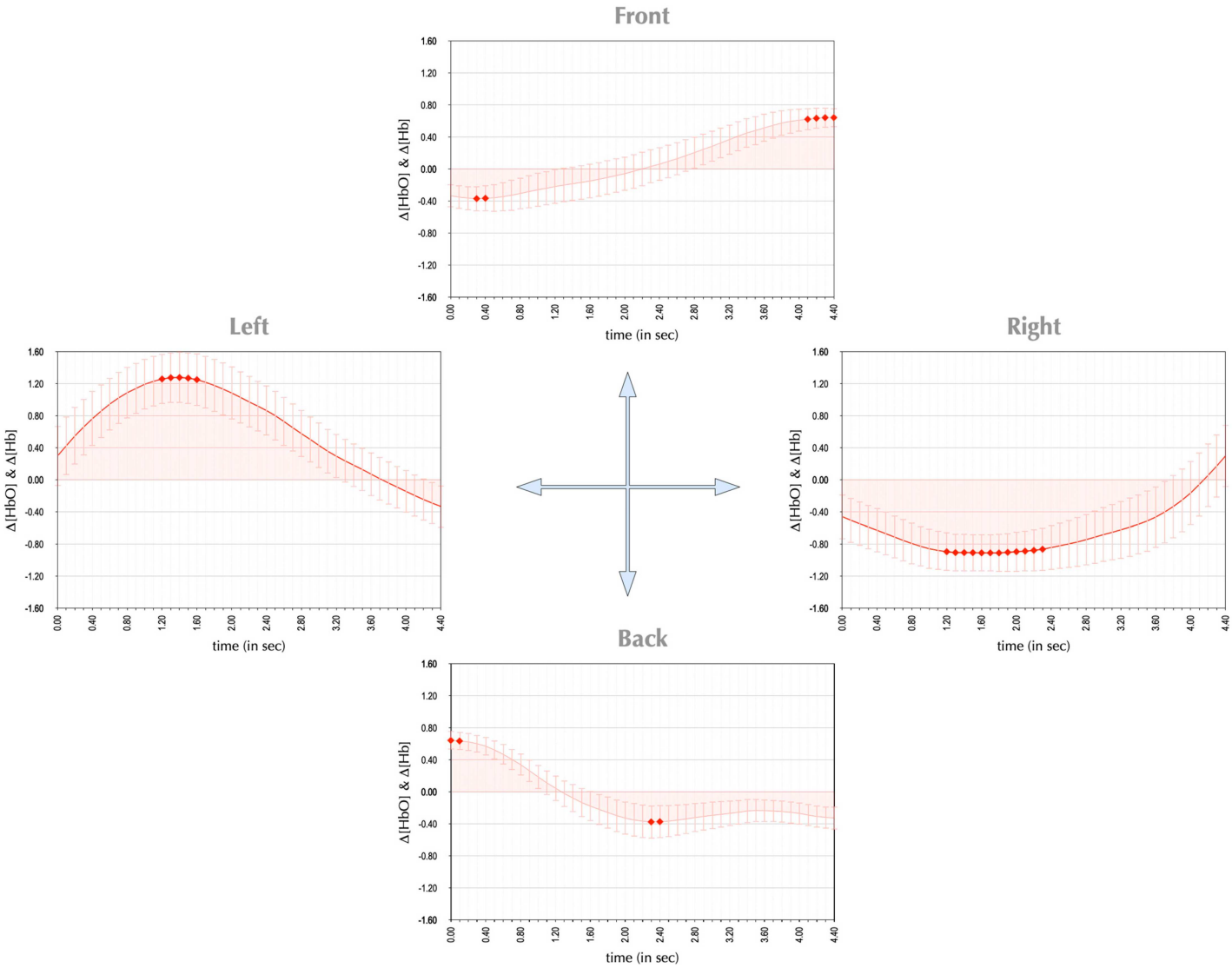

Figure 5 • Average cardio responses (oxy-Hb) during right–left and front–back movements from the same A6 optode shown in **Figure 4**. The right–left tasks exhibited inverse cardio responses for oxygen delivery, peaking to the left and troughing to the right. In contrast, front–back movements demonstrated an increasing slope for forward movements and a decreasing slope for backward movements.

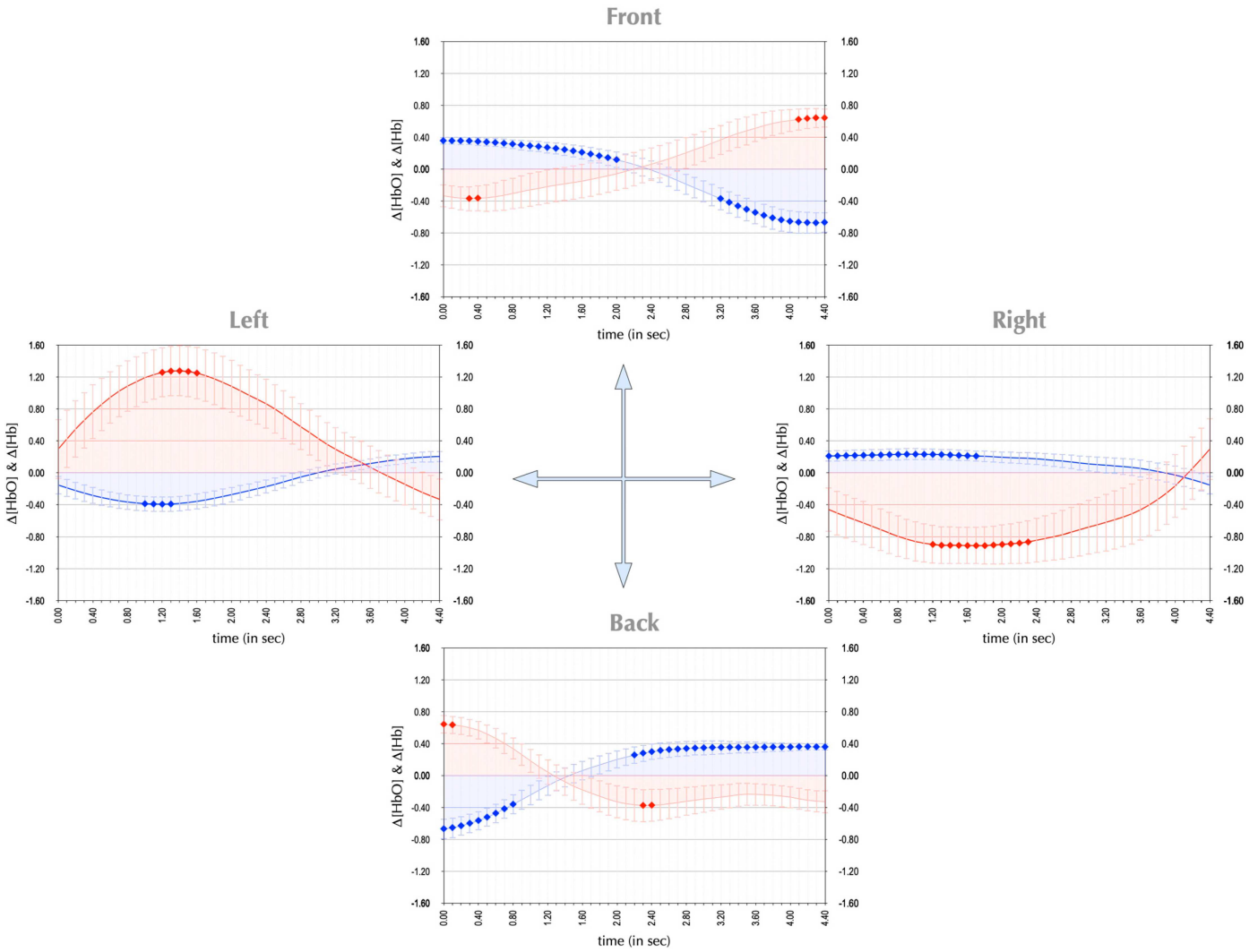

Figure 6 • Hemodynamic responses of oxy-Hb and deoxy-Hb during four orthogonal movements by combining **Figure 4** and **Figure 5** to compare their inverse relationships.

The orientation of the negative diagonal trajectories varies based on right–left and front–back movements. Right–left movements follow an elliptical path (**Figure 8A**). In contrast, front–back movements exhibit a figure-eight pattern (**Figure 8B**). As the hand moves, the hemodynamic relationships change, entering different quadrants of phase space depending on movement direction. Therefore, phase-space trajectory shapes can confirm various orthogonal movement directions.

The phase relationship can identify the direction of opposing movement. **Figure 8A** shows rightward movements (red circles) originating in the second quadrant (oxy-Hb leads deoxy-Hb). In contrast, leftward movements (blue circles) begin in the fourth quadrant (oxy-Hb lags deoxy-Hb). Similarly, **Figure 8B** reveals oxy-Hb leads deoxy-Hb in the second quadrant, initiating forward movements (magenta circles). Conversely, oxy-Hb lags deoxy-Hb in the fourth quadrant at the onset of backward movements (green circles).

4.2.8. Identifying supply and demand bottlenecks

The trajectory orientation angle can differentiate orthogonal movement directions, albeit in an inversely related manner. All trajectories trended negatively along a diagonal due to the physiological inverse relationship between oxy-Hb and deoxy-Hb. However, the orientation angle indicates whether a zero-sum dynamic occurred for that movement direction (see **Figure 7**), in which the availability-to-consumption ratio remained balanced (orientation angle = −1) with constant blood flow during front-back directions (**Figure 8B**). Conversely, a non-zero sum arises when a mismatch between supply and demand—such as vasodilation during leftward movements and vasoconstriction during rightward movements—results in a trajectory orientation angle of less than −1 (**Figure 8A**).

Furthermore, when supply and demand bottleneck, availability falls below consumption, reducing the availability-to-consumption ratio. This occurred in the second quadrant during rightward movements (red circles in **Figure 8A**). The second quadrant indicates an oxygen deficit due to a greater loss in availability compared to the increase in demand, which was limited to rightward movements for identifying movement direction. The total blood volume also decreased during rightward movements, accompanied by vasoconstriction (right graph in **Figure 7**).

In contrast, during leftward movement (blue circles), the trajectory mainly remained in the fourth quadrants, indicating an oxygen surplus as increased availability outpaced decreased consumption. This also coincides with vasodilation (left graph in **Figure 7**). The shift from oxygen deficit to surplus dynamics confirms movement direction based on quadrant location in the phase-space plot.

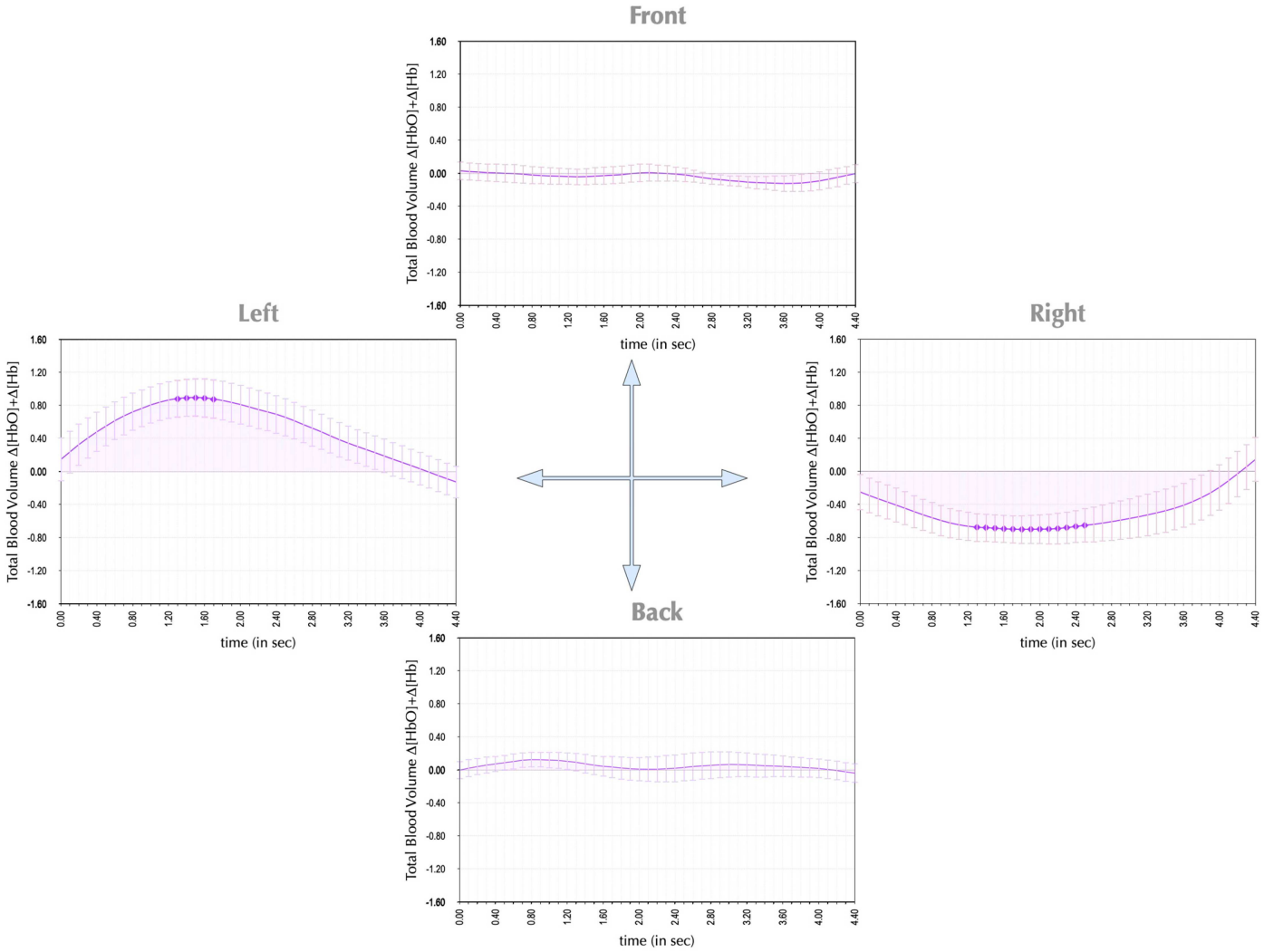

Figure 7 • Graph illustrating changes in total blood volume during movement. The left graph indicates increased volume (vasodilation) during leftward movements, while the right graph shows decreased volume (vasoconstriction) during rightward movements, resulting in non-zero hemodynamic responses. In contrast, the top and bottom graphs depict a constant blood volume during front–back movements, with variations that are not statistically significant compared to the noise levels for zero-sum responses.

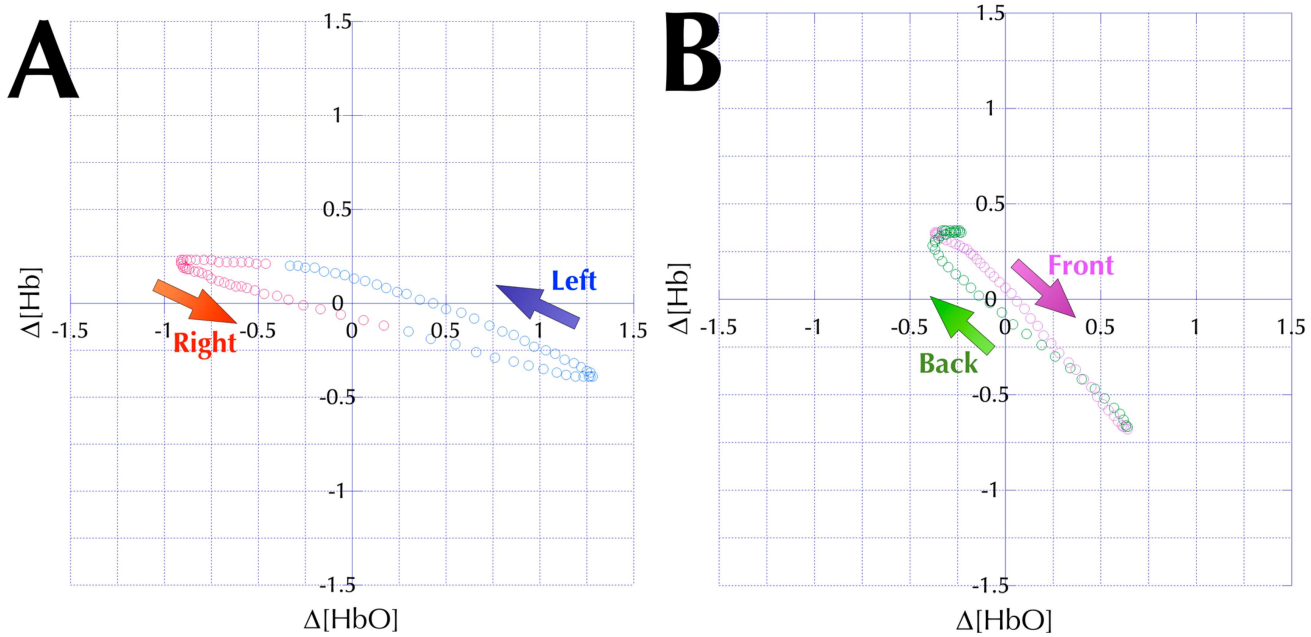

Figure 8 • Phase-space plots illustrate the phase relationships between oxy-Hb and deoxy-Hb levels and movement direction. (**A**) reveals an elliptical pattern for right–left movements and (**B**) shows a figure-eight pattern for front–back movements, both of which are counterclockwise. Trajectories differ along the negative diagonal: right–left movements fall below it, while front–back movements align with it. (Right movements are represented by red circles, left by blue, front by green, and back by magenta.).

5. Discussion

5.1. Direction-specific group firing representations

These results suggest that neighboring neurons within a group recorded under the optode encode similar preferred directions, consistent with other cortical neurons coordinating their firing, such as the visual cortical columns that process similar orientations [57, 58]. Additionally, adjacent neurons process related signals with slight differences [59]. The scalar sum would not show a specific preferred direction if signals were distributed randomly. However, when firing signals exhibit preferred directions—even if they only capture the scalar sum—they can still decode direction if responses are direction-specific. This finding confirms that the PFC encodes direction-specific intentions, while the primary motor cortex manages the execution of movement. Monitoring PFC activity can assist stroke patients with motor cortex damage, as strokes affecting the motor cortex are more prevalent than those in the PFC.

5.2. Multi-hemodynamic variables for decoding

The results illustrate methods for utilizing multiple optical signal representations to ascertain and verify movement direction. The methodology employs derived variables to validate the physiological direction, starting with two independent hemodynamic variables: oxy-Hb and deoxy-Hb. Oxy-Hb signals indicate cardio-responses associated with oxygen delivery, provided that the supply surpasses demand. However, during periods of extreme metabolic activation, demand may outstrip supply, resulting in an oxygen deficit and limitations on oxygen extraction. Deoxy-Hb signals reflect neuro-responses, frequently related to neural activity in reaction to movement directions. Oxy-Hb signals also assist in reconstructing these directions from optical data. Both neuro- and cardio-hemodynamic responses can decode intended movement directions, offering independent metrics for BCI devices. Additional hemodynamic variables, such as blood volume changes and oxygen supply dynamics, could further substantiate decoded directions in tissues.

Even though these additional measures are derived from the independent $\Delta[\mathrm{HbO}]$ and $\Delta[\mathrm{Hb}]$ hemodynamics variables, such as their sum, ratio $\Delta[\mathrm{HbO}]/\Delta[\mathrm{Hb}]$, and phase relationships $(\Delta[\mathrm{HbO}], \Delta[\mathrm{Hb}])$, they are physiologically relevant for validating accuracy. They provide redundant measures for checking the consistency of the decoding algorithm, which is crucial for developing a trustworthy BCI device. Unlike first-generation devices that assume decoding accuracy, the current approach prioritizes failure prevention through various methodologies.

5.3. Movement direction-specific phase-space representations

Previous reports have indicated that oxy-Hb and deoxy-Hb levels vary by movement direction [60, 61]. These neural and cardiovascular variations differentiate responses across directions [56], with changes potentially decoupled during different movements [60, 61]. Current experiments confirmed these dynamics, offering methods to verify movement direction through phase-space analysis of neuro- and cardio responses. Variations reveal differences in neural activity across movements, as illustrated by the earlier phase-space diagram [56].

5.4. Direction-specific total blood volume representations

Experimental evidence shows that oxy-Hb and deoxy-Hb levels vary during motor tasks. The effects may not be zero-sum, depending on the direction of movement. The results indicated vasodilation in one direction and vasoconstriction in the opposite direction, with minimal changes in the orthogonal direction. Thus, hemodynamic responses can validate decoded movement directions from other variables, offering redundant methods for determining movement from optical brain signals.

Deoxy-Hb signals indicate neuro-responses, while oxy-Hb signals reflect cardio responses. Different hemodynamic variables exhibit directional dependence, making multiple measures preferable for decoding movement directions and enhancing decoding accuracy. Oxy-Hb is not always anti-correlated with deoxy-Hb; their relational dynamics vary with direction, which provides verification for decoded movement and boosts confidence in neural representation. Their relationship can be analyzed through phase-space analysis, confirming movement intentions.

5.5. Fault-tolerant BCI designs for fault recovery

Robust engineering design requires fault tolerance, as no machine is perfect. Components can fail due to wear or unforeseen issues, resulting in outages. A well-designed system minimizes these failures and their severe consequences. First-generation BCI devices prioritize accuracy, while second-generation devices focus on mitigating failures. This design incorporates fault-tolerant methods for the graceful degradation of functions, allowing systems to fail and recover smoothly. Such a design is essential for paralyzed patients who cannot physically correct errors in the same way as non-disabled individuals.

The brain-controlled interface may misinterpret movements, necessitating alternative methods to stop the wheelchair without relying on brain signal sensors. One solution is to use voice commands to halt operations, employing existing voice recognition technology in smartphone apps. The software must filter out background noise and recognize specific commands to prevent accidental activations. Although voice control can be cumbersome for wheelchair navigation, it can act as an emergency button to stop operations in urgent situations for users with disabilities.

An alternative method for controlling the wheelchair's direction involves using an accelerometer and gyroscope in the headset to detect tilt and acceleration. Quadriplegic users can nod to confirm movement. However, using head motion as the primary control may result in crashes due to unintentional head movements, such as distractions. Nevertheless, head movement can serve as a secondary confirmation to verify the intended direction before finalizing movements.

5.6. Consistency checking for error detection

The system employs a majority rule to verify actions and integrates a multi-sensor redundant subsystem through a central controller. It checks component accuracy using a consistency-checking scheme. If inconsistencies arise in control signals, the system vetoes the outlier through a majority vote, allowing others to override failures. Voting utilizes a weighted sum to prioritize subsystems, with weights determined by consistency-check statistics, thereby

reducing the probability of failure. Greater sensor reliability translates to higher weights based on accuracy. The likelihood of multiple subsystem failures is lower than that of a single failure, promoting graceful degradation and ongoing operation. Consistency checks help prevent catastrophic failures. An emergency brake is crucial for intervention in subsystem failure, particularly if the user cannot activate a stop button due to headset detachment.

5.7. User-friendly designs and available options for user customization

The system design employs endpoint control to create a more intuitive user experience, eliminating the need for intermediate navigation. Smart car sensors and algorithms autonomously handle path planning and obstacle avoidance using off-the-shelf components, reducing the user's effort and attention when operating the BCI device.

For lightweight headset designs, the BCI controller and battery packs are offloaded to the wheelchair and communicate wirelessly. A helmet design accommodates multiple optodes to monitor signals while blocking infrared interference. A lightweight headband detects PFC activity on the forehead, eliminating interference from hair and providing a budget-friendly alternative to helmets. Users can choose from wireless and wired options based on their budget. These headsets are interchangeable, allowing for easy swapping of components.

5.8. User training and adaptive control

Initial user training is crucial for most systems. Biofeedback shortens the training curve and boosts system accuracy. Neural adaptation manages sensor slippage, much like learning to walk. In addition to detecting head motion tilts and rotations, head motion sensors identify headset slippage caused by sudden acceleration or g-forces, serving as shock sensors during drops. When a headset drops, the system automatically stops wheelchair operations for safety reasons. Headset slippage may misplace detected brain locations for motor decoding, leading to an incorrect interpretation of movement signals. Detecting sensor slippage requires recalibrating brain signals or adapting the decoding algorithm before safely resuming wheelchair operations.

5.9. Practical issues for future considerations

Unlike implants, detectable devices face practical challenges because sensors may shift with head movements. Optodes capture signals from different brain regions when the headset slips, leading to unreliable control. Head motion detectors identify shifts and pause wheelchair operation until the wheelchair is stabilized. Adaptation could assist by recalibrating the system for accurate decoding. Adaptive training may enable the system to learn and refine algorithms to compensate for motion shifts, even though these issues remain unresolved. Users must trust the system's reliability, as individuals with paralysis cannot adjust a slipping headset.

5.10. Applications beyond the original designs

Such BCI devices can assist visually impaired individuals in navigation, help ALS patients communicate or control cursors, provide a hands-free gaming experience without a console, and facilitate military target selection using brain signals. The device may detect if a comatose person is dreaming and communicate with them via the headset. Experiments have shown that comatose patients can respond to instructions for spatial navigation or playing tennis, based on brain activity similar to awake individuals, as indicated by fMRI responses [62, 63]. Their brain activity indicates responses related to motor planning and memory recall. Once implemented, this device will detect and interpret cortical activity for various applications beyond its initial purpose. Such wearable BCI devices offer significant potential beyond navigation in wheelchairs.

6. Conclusions

The results showed that optical PFC neural activities correlated with movement direction, responding oppositely to orthogonal hand movements. The second-generation BCI design anticipates operational failures, providing methodologies to prevent catastrophic failures for safe wheelchair operation. Hemodynamic analyses confirmed direction-specific cortical responses, demonstrating the feasibility of optical imaging in detecting movement intentions for wheelchair control. Direction-specific hemodynamic responses were identified, offering physiologically interpretable validation. This fail-safe wheelchair utilizes a fault-tolerant, multivariable, multi-sensor system for movement detection, integrating multiple hemodynamic variables, head motion, and voice control for redundancy. Multi-sensor integration ensures consistency through voting for control confirmation or rejection and allows for emergency stops with majority verification. It provides a lightweight headband or helmet option to enhance user adoption. Removable optical sensors enable wheelchair operation without implanted electrodes, offering a cost-effective and non-invasive solution. The wired or wireless headset communicates with the wheelchair controller, enabling a detectable and lightweight design for the headset separate from the controller. However, sensor slippage affecting signal detection must be resolved before full-scale commercialization can occur.

Funding

There are no sources of funding to declare.

Author contributions

The author confirms sole responsibility for this work. The author approves of this work and takes responsibility for its integrity.

Conflict of interest

The author declares no conflict of interest.

Data availability statement

Data supporting these findings are available within the article or upon request.

Institutional review board statement

The study was conducted according to the guidelines of the Declaration of Helsinki and approved by the Institutional Review Board

of University of North Texas (protocol code 13457, date of approval 2013 Oct 2).

Informed consent statement

Informed consent was obtained from all subjects involved in the study.

Additional information

Received: 2025-01-09

Accepted: 2025-05-26

Published: 2025-06-25

Academia Engineering papers should be cited as *Academia Engineering 2025*, ISSN 2994-7065, https://doi.org/10.20935/AcadEng7756. The journal's official abbreviation is *Acad. Eng*.

Publisher's note

Copyright

References

1. Schwartz AB. Motor cortical activity during drawing movements: single-unit activity during sinusoid tracing. J Neurophysiol. 1992;68(2):528–41. doi: 10.1152/jn.1992.68.2.528
2. Schwartz AB. Motor cortical activity during drawing movements: population representation during sinusoid tracing. J Neurophysiol. 1993;70(1):28–36. doi: 10.1152/jn.1993.70.1.28
3. Kettner RE, Schwartz AB, Georgopoulos AP. Primate motor cortex and free arm movements to visual targets in three-dimensional space. III. Positional gradients and population coding of movement direction from various movement origins. J Neurosci. 1988;8(8):2938–47. doi: 10.1523/JNEUROSCI.08-08-02938.1988
4. Kettner RE, Marcario JK, Clark-Phelps MC. Control of remembered reaching sequences in monkey. I. Activity during movement in motor and premotor cortex. Exp Brain Res. 1996;112(3):335–46. doi: 10.1007/BF00227940
5. Georgopoulos AP, Kettner RE, Schwartz AB. Primate motor cortex and free arm movements to visual targets in three-dimensional space. II. Coding of the direction of movement by a neuronal population. J Neurosci. 1988;8(8):2928–37. doi: 10.1523/JNEUROSCI.08-08-02928.1988
6. Schwartz AB, Kettner RE, Georgopoulos AP. Primate motor cortex and free arm movements to visual targets in three-dimensional space. I. Relations between single cell discharge and direction of movement. J Neurosci. 1988;8(8):2913–27. doi: 10.1523/JNEUROSCI.08-08-02913.1988
7. Georgopoulos AP, Schwartz AB, Kettner RE. Neuronal population coding of movement direction. Science. 1986;233(4771):1416–9. doi: 10.1126/science.3749885
8. Schwartz AB, Moran DW. Arm trajectory and representation of movement processing in motor cortical activity. Eur J Neurosci. 2000;12(6):1851–6. doi: 10.1046/j.1460-9568.2000.00097.x
9. Schwartz AB. Cortical neural prosthetics. Annu Rev Neurosci. 2004;27:487–507. doi: 10.1146/annurev.neuro.27.070203.144233
10. Golub MD, Yu BM, Schwartz AB, Chase SM. Motor cortical control of movement speed with implications for brain-machine interface control. J Neurophysiol. 2014;112(2):411–29. doi: 10.1152/jn.00391.2013
11. Gaál G. Calculation of movement direction from firing activities of neurons in intrinsic co-ordinate systems defined by their preferred directions. J Theor Biol. 1993;162(1):103–30. doi: 10.1006/jtbi.1993.1079
12. Alahi MEE, Rizu MI, Tina FW, Huang Z, Nag A, Afsarimanesh N. Recent advancements in graphene-based implantable electrodes for neural recording/stimulation. Sensors. 2023;23(24):9911. doi: 10.3390/s23249911
13. Wei W, Wang X. Graphene-based electrode materials for neural activity detection. Materials. 2021;14(20):6170. doi: 10.3390/ma14206170
14. Xu B, Pei J, Feng L, Zhang XD. Graphene and graphene-related materials as brain electrodes. J Mater Chem B. 2021;9(46):9485–96. doi: 10.1039/d1tb01795k
15. Patil AC, Thakor NV. Implantable neurotechnologies: a review of micro- and nanoelectrodes for neural recording. Med Biol Eng Comput. 2016;54(1):23–44. doi: 10.1007/s11517-015-1430-4
16. Värbu K, Muhammad N, Muhammad Y. Past, present, and future of EEG-based BCI applications. Sensors. 2022;22(9):3331. doi: 10.3390/s22093331
17. Plummer C, Harvey AS, Cook M. EEG source localization in focal epilepsy: where are we now? Epilepsia. 2008;49(2):201–18. doi: 10.1111/j.1528-1167.2007.01381.x
18. Bast T, Boppel T, Rupp A, Harting I, Hoechstetter K, Fauser S, et al. Noninvasive source localization of interictal EEG spikes: effects of signal-to-noise ratio and averaging. J Clin Neurophysiol. 2006;23(6):487–97. doi: 10.1097/01.wnp.0000232208.14060.c7

19. Taberna GA, Marino M, Ganzetti M, Mantini D. Spatial localization of EEG electrodes using 3D scanning. J Neural Eng. 2019;16(2):026020. doi: 10.1088/1741-2552/aafdd1

20. Koessler L, Maillard L, Benhadid A, Vignal JP, Braun M, Vespignani H. Spatial localization of EEG electrodes. Neurophysiol Clin. 2007;37(2):97–102. doi: 10.1016/j.neucli.2007.03.002

21. Saibene A, Caglioni M, Corchs S, Gasparini F. EEG-based BCIs on motor imagery paradigm using wearable technologies: a systematic review. Sensors. 2023;23(5):2798. doi: 10.3390/s23052798

22. Padfield N, Zabalza J, Zhao H, Masero V, Ren J. EEG-based brain-computer interfaces using motor-imagery: techniques and challenges. Sensors. 2019;19(6):1423. doi: 10.3390/s19061423

23. Fok S, Schwartz R, Wronkiewicz M, Holmes C, Zhang J, Somers T, et al. An EEG-based brain computer interface for rehabilitation and restoration of hand control following stroke using ipsilateral cortical physiology. Annu Int Conf IEEE Eng Med Biol Soc. 2011;2011:6277–80. doi: 10.1109/IEMBS.2011.6091549

24. Fleury M, Figueiredo P, Vourvopoulos A, Lécuyer A. Two is better? Combining EEG and fMRI for BCI and neurofeedback: a systematic review. J Neural Eng. 2023;20(5):051003. doi: 10.1088/1741-2552/ad06e1

25. Volkova K, Lebedev MA, Kaplan A, Ossadtchi A. Decoding movement from electrocorticographic activity: a review. Front Neuroinform. 2019;13:74. doi: 10.3389/fninf.2019.00074

26. Śliwowski M, Martin M, Souloumiac A, Blanchart P, Aksenova T. Decoding ECoG signal into 3D hand translation using deep learning. J Neural Eng. 2022;19(2):026023. doi: 10.1088/1741-2552/ac5d69

27. Wang W, Collinger JL, Degenhart AD, Tyler-Kabara EC, Schwartz AB, Moran DW, et al. An electrocorticographic brain interface in an individual with tetraplegia. PLoS One. 2013;8(2):e55344. doi: 10.1371/journal.pone.0055344

28. Hillman EMC. Coupling mechanism and significance of the BOLD signal: a status report. Annu Rev Neurosci. 2014;37:161–81. doi: 10.1146/annurev-neuro-071013-014111

29. Rector DM, Yao X, Harper RM, George JS. In vivo observations of rapid scattered light changes associated with neurophysiological activity. In: Frostig RD, editor. In vivo optical imaging of brain function. 2nd ed. Boca Raton (FL): CRC Press/Taylor & Francis; 2009. Available from: https://www.ncbi.nlm.nih.gov/books/NBK20228/

30. Kocsis L, Herman P, Eke A. The modified Beer-Lambert law revisited. Phys Med Biol. 2006;51(5):N91–8. doi: 10.1088/0031-9155/51/5/N02

31. Baker WB, Parthasarathy AB, Busch DR, Mesquita RC, Greenberg JH, Yodh AG. Modified Beer-Lambert law for blood flow. Biomed Opt Express. 2014;5(11):4053–75. doi: 10.1364/BOE.5.004053

32. Bashkatov AN, Genina EA, Kochubey VI, Tuchin VV. Optical properties of human skin, subcutaneous and mucous tissues in the wavelength range from 400 to 2000 nm. J Phys D Appl Phys. 2005;38(15):2543. doi: 10.1088/0022-3727/38/15/004

33. Chan ED, Chan MM, Chan MM. Pulse oximetry: Understanding its basic principles facilitates appreciation of its limitations. Respir Med. 2013;107(6):789–99. doi: 10.1016/j.rmed.2013.02.004

34. He Q, Sun Z, Li Y, Wang W, Wang RK. Spatiotemporal monitoring of changes in oxy/deoxy-hemoglobin concentration and blood pulsation on human skin using smartphone-enabled remote multispectral photoplethysmography. Biomed Opt Express. 2021;12(5):2919–37. doi: 10.1364/BOE.423160

35. Ayaz H, Baker WB, Blaney G, Boas DA, Bortfeld H, Brady K, et al. Optical imaging and spectroscopy for the study of the human brain: status report. Neurophotonics. 2022;9(Suppl 2):S24001. doi: 10.1117/1.NPh.9.S2.S24001

36. Steinbrink J, Wabnitz H, Obrig H, Villringer A, Rinneberg H. Determining changes in NIR absorption using a layered model of the human head. Phys Med Biol. 2001;46(3):879–96. doi: 10.1088/0031-9155/46/3/320

37. Obrig H, Villringer A. Beyond the visible—imaging the human brain with light. J Cereb Blood Flow Metab. 2003;23(1):1–18. doi: 10.1097/01.WCB.0000043472.45775.29

38. Cui X, Bray S, Bryant DM, Glover GH, Reiss AL. A quantitative comparison of NIRS and fMRI across multiple cognitive tasks. Neuroimage. 2011;54(4):2808–21. doi: 10.1016/j.neuroimage.2010.10.069

39. Liu N, Cui X, Bryant DM, Glover GH, Reiss AL. Inferring deep-brain activity from cortical activity using functional near-infrared spectroscopy. Biomed Opt Express. 2015;6(3):1074–89. doi: 10.1364/BOE.6.001074

40. Scholkmann F, Kleiser S, Metz AJ, Zimmermann R, Mata Pavia J, Wolf U, et al. A review on continuous wave functional near-infrared spectroscopy and imaging instrumentation and methodology. Neuroimage. 2014;85(Pt1):6–27. doi: 10.1016/j.neuroimage.2013.05.004

41. Delpy DT, Arridge SR, Cope M, Edwards D, Reynolds EO, Richardson CE, et al. Quantitation of pathlength in optical spectroscopy. Adv Exp Med Biol. 1989;248:41–6. doi: 10.1007/978-1-4684-5643-1_5

42. Del Bianco S, Martelli F, Zaccanti G. Penetration depth of light re-emitted by a diffusive medium: theoretical and experimental investigation. Phys Med Biol. 2002;47(23):4131–44. doi: 10.1088/0031-9155/47/23/301

43. Naseer N, Hong KS. fNIRS-based brain-computer interfaces: a review. Front Hum Neurosci. 2015;9:3. doi: 10.3389/fnhum.2015.00003

44. Chen J, Xia Y, Zhou X, Vidal Rosas E, Thomas A, Loureiro R, et al. fNIRS-EEG BCIs for motor rehabilitation: a review. Bioengineering. 2023;10(12):1393. doi: 10.3390/bioengineering10121393

45. Ahn S, Jun SC. Multi-Modal Integration of EEG-fNIRS for brain-computer interfaces-current limitations and future directions. Front Hum Neurosci. 2017;11:503. doi: 10.3389/fnhum.2017.00503

46. Li C, Zhu Y, Qu W, Sun L. Research on blood oxygen activity in cerebral cortical motor function areas with adjustment intention during gait. Technol Health Care. 2021;29(4):677–86. doi: 10.3233/THC-202580

47. Hong KS, Khan MJ, Hong MJ. Feature extraction and classification methods for hybrid fNIRS-EEG brain-computer interfaces. Front Hum Neurosci. 2018;12:246. doi: 10.3389/fnhum.2018.00246

48. Nazeer H, Naseer N, Khan RA, Noori FM, Qureshi NK, Khan US, et al. Enhancing classification accuracy of fNIRS-BCI using features acquired from vector-based phase analysis. J Neural Eng. 2020;17(5):056025. doi: 10.1088/1741-2552/abb417

49. Asgher U, Khan MJ, Asif Nizami MH, Khalil K, Ahmad R, Ayaz Y, et al. Motor training using mental workload (MWL) with an assistive soft exoskeleton system: a functional near-infrared spectroscopy (fNIRS) study for brain-machine interface (BMI). Front Neurorobot. 2021;15:605751. doi: 10.3389/fnbot.2021.605751

50. Floreani ED, Orlandi S, Chau T. A pediatric near-infrared spectroscopy brain-computer interface based on the detection of emotional valence. Front Hum Neurosci. 2022;16:938708. doi: 10.3389/fnhum.2022.938708

51. Bak S, Jeong Y, Yeu M, Jeong J. Brain-computer interface to predict impulse buying behavior using functional near-infrared spectroscopy. Sci Rep. 2022;12(1):18024. doi: 10.1038/s41598-022-22653-8

52. Page ES. Continuous inspection schemes. Biometrika. 1954;41(1/2):100–15. doi: 10.2307/2333009

53. Tam D. A theoretical analysis of cumulative sum slope (CUSUM-slope) statistic for detecting signal onset (begin) and offset (end) trends from background noise level. Open Math Stat Probab J. 2009;1(1):43–51. doi: 10.2174/1876527000901010043

54. Tam DC. A Multi-Neuronal Vectorial Phase-Space Analysis for Detecting Dynamical Interactions in Firing Patterns of Biological Neural Networks. In: Eeckman FH, Bower JM, editors. Computation and Neural Systems. Boston (MA): Springer US; 1993. p. 49–53. doi: 10.1007/978-1-4615-3254-5_8

55. Tam DC. Vectorial phase-space analysis for detecting dynamical interactions in firing patterns of biological neural networks. Proceedings of the IJCNN International Joint Conference on Neural Networks [Proceedings 1992]; 1992 Jun 7–11; Piscataway (NJ): IEEE; 1992. p. 97–102. doi: 10.1109/IJCNN.1992.227184

56. Tam N, Pollonini L, Zouridakis G. Decoding movement direction using phase-space analysis of hemodynamic responses to arm movements based on functional near-infrared spectroscopy. Annu Int Conf IEEE Eng Med Biol Soc. 2016:1580–3. doi: 10.1109/EMBC.2016.7591014

57. Hubel DH, Wiesel TN. Visual area of the lateral suprasylvian gyrus (Clare-Bishop area) of the cat. J Physiol. 1969;202(1):251–60. doi: 10.1113/jphysiol.1969.sp008808

58. Hubel DH, Wiesel TN. Receptive fields and functional architecture of monkey striate cortex. J Physiol. 1968;195(1):215–43. doi: 10.1113/jphysiol.1968.sp008455

59. Hubel DH, Wiesel TN. Sequence regularity and geometry of orientation columns in the monkey striate cortex. J Comp Neurol. 1974;158(3):267–93. doi: 10.1002/cne.901580304

60. Tam ND, Zouridakis G. Decoding movement direction from motor cortex recordings using near-infrared spectroscopy. In: Infrared spectroscopy: theory, developments and applications. Hauppauge (NY): Nova Science Publishers, Inc.; 2014. p. 189–201. [cited 2014 Jan 1]. Available from: https://www.scopus.com/inward/record.uri?eid=2-s2.0-84953222346&partnerID=40&md5=55656b144ed9e55268f9162b61fd1165

61. Tam ND, Zouridakis G. Differential temporal activation of oxy- and deoxy-hemodynamic signals in optical imaging using functional near-infrared spectroscopy (fNIRS). BMC Neurosci. 2015;16(1):P245. doi: 10.1186/1471-2202-16-S1-P245

62. Owen AM, Coleman MR, Boly M, Davis MH, Laureys S, Pickard JD. Detecting awareness in the vegetative state. Science. 2006;313(5792):1402. doi: 10.1126/science.1130197

63. Owen AM, Coleman MR. Detecting awareness in the vegetative state. Ann N Y Acad Sci. 2008;1129:130–8. doi: 10.1196/annals.1417.018